

Excitons in solids from periodic equation-of-motion coupled-cluster theory

Xiao Wang¹ and Timothy C. Berkelbach^{1,2,*}

¹*Center for Computational Quantum Physics, Flatiron Institute, New York, New York 10010 USA*

²*Department of Chemistry, Columbia University, New York, New York 10027 USA*

We present an ab initio study of electronically excited states of three-dimensional solids using Gaussian-based periodic equation-of-motion coupled-cluster theory with single and double excitations (EOM-CCSD). The explicit use of translational symmetry, as implemented via Brillouin zone sampling and momentum conservation, is responsible for a large reduction in cost. Our largest system studied, which samples the Brillouin zone using 64 k -points (a $4 \times 4 \times 4$ mesh) corresponds to a canonical EOM-CCSD calculation of 768 electrons in 640 orbitals. We study eight simple semiconductors and insulators, with direct singlet excitation energies in the range of 3 to 15 eV. Our predicted excitation energies exhibit a mean absolute error of 0.27 eV when compared to experiment. We furthermore calculate the energy of excitons with nonzero momentum and compare the exciton dispersion of LiF with experimental data from inelastic X-ray scattering. By calculating excitation energies under strain, we extract hydrostatic deformation potentials in order to quantify the strength of interactions between excitons and acoustic phonons. Our results indicate that coupled-cluster theory is a promising method for the accurate study of a variety of exciton phenomena in solids.

I. INTRODUCTION

Density functional theory (DFT) is the workhorse of computational materials science and commonly predicts ground-state properties with high accuracy.¹⁻⁸ Extending this success to the prediction of excited-state properties is an ongoing challenge. Time-dependent DFT (TDDFT)⁹ struggles to treat neutral excitations in the condensed phase and reasonable accuracy requires the use of hybrid functionals and/or frequency-dependent exchange-correlation kernels.¹⁰⁻²⁰ Instead, the community typically builds upon DFT through Green's function-based many-body perturbation theory.¹³ For weakly-correlated materials, including simple metals, semiconductors, and insulators, the GW approximation to the self-energy²¹⁻²⁶ combined with the same approximation to the Bethe-Salpeter equation²⁷⁻³¹ yields excited state properties that are typically in good agreement with experiment. Strongly-correlated materials are more commonly treated via dynamical mean-field theory (DMFT),^{32,33} either in the DFT+DMFT framework³⁴⁻³⁶ or the GW+DMFT framework.^{37,38} Alternatively, quantum Monte Carlo methods have been adapted for the calculation of excitation energies, including variational³⁹ and diffusion Monte Carlo⁴⁰⁻⁴² and auxiliary-field quantum Monte Carlo.⁴³

In recent years, wavefunction-based techniques from the quantum chemistry community have been adapted for periodic boundary conditions and applied to condensed-phase systems. For ground-state properties, we mention the application of Møller-Plesset perturbation theory,⁴⁴⁻⁴⁷ coupled-cluster theory,⁴⁸⁻⁵² and – for small supercells – full configuration interaction quantum Monte Carlo.⁵³ Charged excitation energies, as quantified through the one-particle spectral function or the band structure, have been studied by periodic equation-of-motion coupled-cluster theory for the uniform electron gas,⁵⁴ for the simple semiconductors silicon and diamond,⁵² for two-dimensional MoS₂,⁵⁵ and for transition metal oxides.⁵⁶

Neutral excitation energies have been primarily studied by configuration interaction with single excitations (CIS),^{57,58}

which is equivalent to the use of the Hartree-Fock self-energy in the Bethe-Salpeter equation (with the Tamm-Dancoff approximation). Due to the unscreened nature of the Coulomb interaction, periodic CIS typically predicts excitation energies which are much too large.⁵⁹ Recently, periodic equation-of-motion coupled-cluster theory with single and double excitations (EOM-CCSD) was applied to one-dimensional polyethylene in a small single-particle basis set,⁵⁰ producing results in reasonable agreement with experiment. For three-dimensional condensed-phase systems, our group has recently applied EOM-CCSD to the neutral excited-state properties of the uniform electron gas⁶⁰ as well as the absorption and pump-probe spectroscopy of the naphthalene crystal at the Γ point.⁶¹

Here, we continue this endeavor and present the results of a new EOM-CCSD implementation with translational symmetry and Brillouin zone sampling for three-dimensional atomic solids. The layout of the article is as follows. In section II, we describe the theory underlying our implementation, including details about our symmetry-adapted Gaussian basis sets and periodic EOM-CCSD. In section III, we present computational details, including details about the materials studied, the basis sets used, and integral evaluation. In section IV, we provide EOM-CCSD results on the excitation energies (including a comparison with CIS and a discussion of finite-size effects), the exciton binding energy, the dispersion of excitons with nonzero momentum, and the exciton-phonon interaction. In section V, we summarize our results and conclude with future directions.

II. THEORY

Our periodic calculations are performed using a translational-symmetry-adapted single-particle basis,

$$\phi_{\mu\mathbf{k}}(\mathbf{r}) = \sum_{\mathbf{T}} e^{i\mathbf{k}\cdot\mathbf{T}} \tilde{\phi}_{\mu}(\mathbf{r} - \mathbf{T}), \quad (1)$$

where $\tilde{\phi}_{\mu}(\mathbf{r})$ is an atom-centered Gaussian orbital, \mathbf{T} is a lattice translation vector, and \mathbf{k} is a crystal momentum vector

sampled from the first Brillouin zone. A Hartree-Fock calculation in this basis produces crystalline orbitals (COs)

$$\psi_{p\mathbf{k}}(\mathbf{r}) = \sum_{\mu} C_{\mu p}(\mathbf{k}) \phi_{\mu\mathbf{k}}(\mathbf{r}), \quad (2)$$

where p is the band index and $C_{\mu p}(\mathbf{k})$ are the CO coefficients.

The periodic CCSD energy and cluster amplitudes are determined by the usual equations,^{49,62–66}

$$E_0 = \langle \Phi_0 | \bar{H} | \Phi_0 \rangle, \quad (3)$$

$$0 = \langle \Phi_{ik_i}^{ak_a} | \bar{H} | \Phi_0 \rangle, \quad (4)$$

$$0 = \langle \Phi_{ik_ijk_j}^{ak_abk_b} | \bar{H} | \Phi_0 \rangle, \quad (5)$$

where $\Phi_{ik_i}^{ak_a}$ and $\Phi_{ik_ijk_j}^{ak_abk_b}$ are Slater determinants with one and two electron-hole pairs, indices i, j, k, l denote occupied orbitals, and a, b, c, d denote virtual orbitals. The similarity transformed Hamiltonian is given by $\bar{H} \equiv e^{-T} H e^T$, where $T = T_1 + T_2$ is a momentum-conserving cluster operator with

$$T_1 = \sum_{ai} \sum'_{\mathbf{k}_a \mathbf{k}_i} t_{ik_i}^{ak_a} a_{ak_a}^{\dagger} a_{ik_i}, \quad (6)$$

$$T_2 = \frac{1}{4} \sum_{abij} \sum'_{\mathbf{k}_a \mathbf{k}_b \mathbf{k}_i \mathbf{k}_j} t_{ik_ijk_j}^{ak_abk_b} a_{ak_a}^{\dagger} a_{bk_b}^{\dagger} a_{jk_j} a_{ik_i}. \quad (7)$$

The primed summations indicate momentum conservation.

Excited states are accessed in coupled-cluster theory using the equation-of-motion (EOM) formalism,^{66–71} which amounts to diagonalizing the effective Hamiltonian \bar{H} in a truncated space of excitations. For neutral excitations considered in this work, we use electronic excitation (EE) EOM-CCSD, where the diagonalization is performed in the basis of 1-particle+1-hole and 2-particle+2-hole states. We study excitations with zero and nonzero momentum \mathbf{q} by using a basis of determinants with the corresponding momentum. The (right-hand) excited state is therefore given by

$$|\Psi(\mathbf{q})\rangle = [R_1(\mathbf{q}) + R_2(\mathbf{q})] e^T |\Phi_0\rangle \quad (8)$$

with

$$R_1(\mathbf{q}) = \sum_{ai} \sum'_{\mathbf{k}_a \mathbf{k}_i} r_{ik_i}^{ak_a} a_{ak_a}^{\dagger} a_{ik_i}, \quad (9)$$

$$R_2(\mathbf{q}) = \frac{1}{4} \sum_{abij} \sum'_{\mathbf{k}_a \mathbf{k}_b \mathbf{k}_i \mathbf{k}_j} r_{ik_ijk_j}^{ak_abk_b} a_{ak_a}^{\dagger} a_{bk_b}^{\dagger} a_{jk_j} a_{ik_i}, \quad (10)$$

where the primed summations indicate that the momenta sum to \mathbf{q} . The use of translational symmetry in CCSD leads to a computational cost that scales like $o^2 v^4 N_k^4$, where o is the number of occupied orbitals per unit cell, v is the number of virtual orbitals per unit cell, and N_k is the number of k -points sampled. Further details about periodic Gaussian-based Hartree-Fock and CCSD can be found in Ref. 52.

III. COMPUTATIONAL DETAILS

We study eight semiconducting and insulating materials featuring the diamond/zinc-blende crystal structure and the

rock salt crystal structure. The materials have a wide range of both direct and indirect band gaps and a variety of ionic and covalent bonding. The eight materials and the lattice constants used are given in Tab. I. In all calculations, the Brillouin zone was sampled with a uniform Monkhorst-Pack mesh⁷² of N_k k -points that includes the Γ point.

Our calculations are performed with GTH pseudopotentials,^{73,74} although we perform some all-electron calculations for comparison. For pseudopotential calculations, we use the corresponding polarized double- and triple-zeta basis sets DZVP and TZVP.⁷⁵ For all-electron calculations, we use a modification of the cc-pVDZ basis set presented in Ref. 59, denoted AE-PVDZ.

The finite-size errors of periodic calculations are influenced by the treatment of two-electron repulsion integrals (ERIs). Many of these integrals are formally divergent, due to the long-range nature of the Coulomb interaction; however, these divergent ERIs enter into expressions for observables as integrable divergences, producing well-defined results in the thermodynamic limit. In order to avoid divergent ERIs, we calculate all atomic orbital ERIs as

$$(\mu\mathbf{k}_{\mu}, \nu\mathbf{k}_{\nu} | \kappa\mathbf{k}_{\kappa}, \lambda\mathbf{k}_{\lambda}) = N_k^{-1} \int d\mathbf{r}_1 \int d\mathbf{r}_2 \frac{\rho_{\mu\nu}^{\mathbf{k}_{\mu}\mathbf{k}_{\nu}}(\mathbf{r}_1) \rho_{\kappa\lambda}^{\mathbf{k}_{\kappa}\mathbf{k}_{\lambda}}(\mathbf{r}_2)}{|\mathbf{r}_1 - \mathbf{r}_2|}, \quad (11)$$

where the orbital-pair densities have had their net charge removed,

$$\rho_{\mu\nu}^{\mathbf{k}_{\mu}\mathbf{k}_{\nu}}(\mathbf{r}) = \phi_{\mu\mathbf{k}_{\mu}}^*(\mathbf{r}) \phi_{\nu\mathbf{k}_{\nu}}(\mathbf{r}) - \bar{\rho}_{\mu\nu}, \quad (12a)$$

$$\bar{\rho}_{\mu\nu} = \frac{1}{N_k \Omega} \int d\mathbf{r} \phi_{\mu\mathbf{k}_{\mu}}^*(\mathbf{r}) \phi_{\nu\mathbf{k}_{\nu}}(\mathbf{r}), \quad (12b)$$

and Ω is the volume of the unit cell. The ERIs are then calculated using periodic Gaussian density fitting with an even-tempered auxiliary basis as described in Ref. 76. We note that the use of chargeless pair densities is equivalent to neglecting the $\mathbf{G} = 0$ component of the ERIs when calculated in a plane-wave basis. At the HF level, this treatment of ERIs produces an energy that converges to the thermodynamic limit as $N_k^{-1/3}$, due to the exchange energy; this can be corrected with a Madelung constant, leading to N_k^{-1} convergence.^{77,78} This particular finite-size behavior is also present in the occupied orbital energies $\varepsilon_i(\mathbf{k})$.

We use a closed-shell implementation of periodic EOM-CCSD and study singlet excitations in this work, which are calculated by Davidson diagonalization.^{79,80} The initial guess used in the iterative diagonalization is obtained from dense diagonalization of the effective Hamiltonian in the single excitation subspace.

All calculations were performed with the open-source PySCF software package.⁸¹

IV. RESULTS AND DISCUSSION

A. Direct optical excitation energy

In this section, we study the performance of periodic EOM-CCSD on the lowest-lying direct singlet excitation energies

for the eight selected solids. Such states are relevant for absorption spectroscopy where no momentum is transferred during excitation.

In periodic electronic structure calculations, it is desirable to achieve convergence with respect to the single-particle basis set, the level of correlation, and Brillouin zone sampling. The first two categories have been widely studied in molecular systems and the convergence behavior of the third one is well understood at the mean-field level.^{78,82,83} However, at the correlated level, it is still an open question how to efficiently converge the Brillouin zone sampling in order to reach the thermodynamic limit.^{51,84–86}

1. CIS

As a warm-up to EOM-CCSD, we first present results for periodic configuration interaction with single excitations (CIS), which forms a minimal theory for electronic excited states in the condensed phase. Importantly, the relatively low cost of CIS allows us to study the convergence with respect to Brillouin zone sampling up to relatively large k -point meshes (either 7^3 or 8^3).

The finite-size error of the CIS excitation energy can be analyzed approximately by considering it as the difference between the energy of two determinants, the HF one $|\Phi_0\rangle$ and a single excitation $|\Phi_{ik}^{ak}\rangle$. As discussed above, the energy of a single determinant calculated using our handling of ERIs exhibits a finite-size error decaying like $N_k^{-1/3}$, but which can be removed by a Madelung constant that depends only on the number of electrons in the unit cell. Therefore, the correction is identical for both states, and this leading-order error cancels in the energy difference. We thus posit that the CIS energy converges at least as fast as N_k^{-1} .

In Fig. 1, we show the excitation energy predicted by CIS for the LiF crystal as a function of N_k^{-1} . Clearly, the finite-size error decays at least as fast as N_k^{-1} and so we use the three-parameter fitting function

$$E(N_k) = E_\infty + a N_k^{-1} + b N_k^{-2}, \quad (13)$$

in order to extrapolate to the thermodynamic limit ($N_k \rightarrow \infty$). This fit is shown by the dashed line in Fig. 1, which includes results between 3^3 and 7^3 k -points.

Using an all-electron double-zeta basis set, we performed CIS calculations on a subset of our eight materials, in order to compare to previously published CIS results from Lorenz et al.⁵⁹ By extrapolation of our results obtained at large k -point meshes using the above form, we obtain converged excitation energies (the ‘‘AE-PVDZ/Conv’’ column of Tab. I) that are within 0.1 eV of Ref. 59 for all materials studied. However, we emphasize that the CIS excitation energies are larger than experiment by 2 eV or more.

Before moving on to our EOM-CCSD results, we use CIS to assess some of the future approximations we will have to make. In particular, we will only access k -point meshes up to $4 \times 4 \times 4$ and we will use GTH pseudopotentials and corresponding DZVP basis sets. First, considering finite-size er-

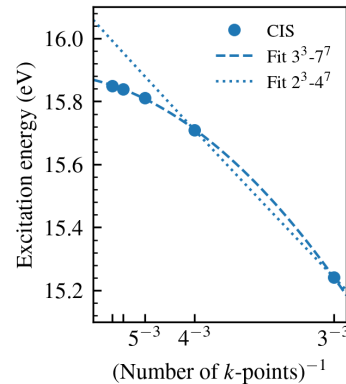


FIG. 1. Excitation energy of LiF calculated with CIS using the DZVP basis set. The dashed line is a fit to results obtained with a number of k -points between 3^3 and 7^3 . The dotted line includes only 2^3 , 3^3 , and 4^3 k -points.

rors, we re-fit the CIS data using the same form but excluding all k -point meshes larger than $4 \times 4 \times 4$; for LiF, the result of this fit is shown as the dotted line in Fig. 1. Clearly, without larger k -point meshes, this extrapolation predicts an excitation energy which is too high by about 0.2 eV. These limited extrapolation results are shown for all materials in the ‘‘AE-PVDZ/234-Extrap’’ column of Tab. I and exhibit errors of about ± 0.5 eV. Second, considering pseudopotential errors, in the last two columns of Tab. I, we show the excitation energies calculated with GTH pseudopotentials. In many cases, the pseudopotential error is less than 0.1 eV; naturally, materials containing heavier second-row atoms such as Si or Mg exhibit the largest errors, which are about 0.3 eV.

2. EOM-CCSD

We now move on to our results from periodic EOM-CCSD. Again, due to the high cost of these calculations, we uti-

TABLE I. Singlet excitation energies (eV) from all-electron and pseudopotential-based periodic CIS

| System | a (Å) | AE-PVDZ | | | DZVP | |
|---------|---------|-------------------------|-------------------|---------|-------------------------|-------------------|
| | | 234-Extrap ^a | Conv ^b | Ref. 59 | 234-Extrap ^a | Conv ^b |
| Diamond | 3.567 | 10.99 | 11.76 | 11.72 | 11.07 | 11.81 |
| Si | 5.431 | 5.84 | 6.14 | 6.05 | 5.43 | 5.71 |
| SiC | 4.360 | 9.41 | 9.83 | 9.74 | 9.12 | 9.47 |
| LiF | 3.990 | 16.02 | 15.85 | 15.84 | 16.06 | 15.87 |
| LiCl | 5.130 | | | | 11.04 | 10.89 |
| MgO | 4.213 | 12.00 | 11.91 | 11.94 | 11.69 | 11.66 |
| BN | 3.615 | | | | 14.17 | 14.32 |
| AlP | 5.451 | | | | 6.59 | 6.76 |

^a Extrapolation based on results obtained with 2^3 , 3^3 , and 4^3 k -point meshes

^b Extrapolation based on results obtained with 3^3 up to 7^3 k -point meshes

TABLE II. Singlet excitation energies (eV) from periodic EOM-CCSD

| System | 234-Extrap ^a | Δ_{frz}^b | ΔTZ^c | Final | Expt. |
|---------|-------------------------|-------------------------|---------------------|-------|---|
| Diamond | 7.70 | -0.18 | -0.05 | 7.47 | 7.3 ⁸⁷ |
| Si | 3.96 | -0.37 | -0.07 | 3.52 | 3.4 ⁸⁸ |
| SiC | 6.53 | -0.19 | -0.08 | 6.27 | 6.0 ⁸⁹ |
| LiF | 14.29 | -0.82 | +0.01 ^d | 13.48 | 12.7, ⁹⁰ 13.68 ⁹¹ |
| LiCl | 9.62 | -0.27 | -0.07 | 9.29 | 8.9 ⁹² |
| MgO | 8.55 | -0.19 | -0.07 | 8.29 | 7.6 ⁹³ |
| BN | 11.48 | -0.35 | -0.02 | 11.11 | 11 ⁹⁴ |
| AIP | 4.97 | -0.42 | -0.07 | 4.48 | 4.6 ^{95,96} |
| MSE | | | | 0.24 | |
| MAE | | | | 0.27 | |

^a Extrapolation based on frozen-virtual DZVP results obtained with 2^3 , 3^3 , and 4^3 k -point meshes

^b Δ_{frz} is the energy difference between complete DZVP and frozen-virtual DZVP on a $3 \times 3 \times 3$ k -point grid

^c ΔTZ is the energy difference between TZVP and DZVP on a $2 \times 2 \times 2$ k -point grid

^d For LiF, the TZVP basis set has severe linear dependencies and was modified by doubling the exponents of the two most diffuse s- and p-type primitive Gaussian functions of Li (all basis functions of F are unchanged)

lized GTH pseudopotentials, sampled the Brillouin zone with meshes up to $4 \times 4 \times 4$, and used basis set corrections. In particular, our primary calculations were based on a HF reference obtained with the full DZVP basis set; subsequent CCSD and EOM-CCSD calculations then employed frozen virtual orbitals, typically correlating 4 lowest virtual bands. The results of these calculations were used to extrapolate to the thermodynamic limit using the same empirical formula as described above (Eq. 13). These results are given in the “234-Extrap” column of Tab. II. To these values, we then added two basis set corrections, Δ_{frz} and ΔTZ ; Δ_{frz} is the energy difference between complete and frozen-orbital DZVP calculations with a $3 \times 3 \times 3$ k -point mesh; ΔTZ is the energy difference between TZVP and DZVP calculations with a $2 \times 2 \times 2$ k -point mesh. Whereas Δ_{frz} is typically between 0.2 and 0.8 eV, ΔTZ is less than 0.1 eV.

Basis-set corrected excitation energies as a function of N_k^{-1} are shown in Figure 2 for diamond, Si, LiF, and MgO. Our final values for all eight materials are given in the “Final” column of Tab. II and compared to experiment. Unsurprisingly, EOM-CCSD is a massive improvement over CIS; for the eight solids studied here, EOM-CCSD predicts excitation energies with a mean signed error (MSE) of 0.24 eV and a mean absolute error (MAE) of 0.27 eV.

A few results in Tab. II are noteworthy. First, we note that the excitation energy of cubic BN is frequently reported as 6.4 eV, which is almost 5 eV lower than the EOM-CCSD prediction. However, a GW/BSE calculation reported in 2004⁹⁷ also found a value of around 11 eV and proposed a reinterpretation of the experimental data. Indeed, a joint theory-experiment paper published in 2018⁹⁴ attributed the lower energy absorption features to a combination of defects and domains of hexagonal BN, further supporting a direct excitation

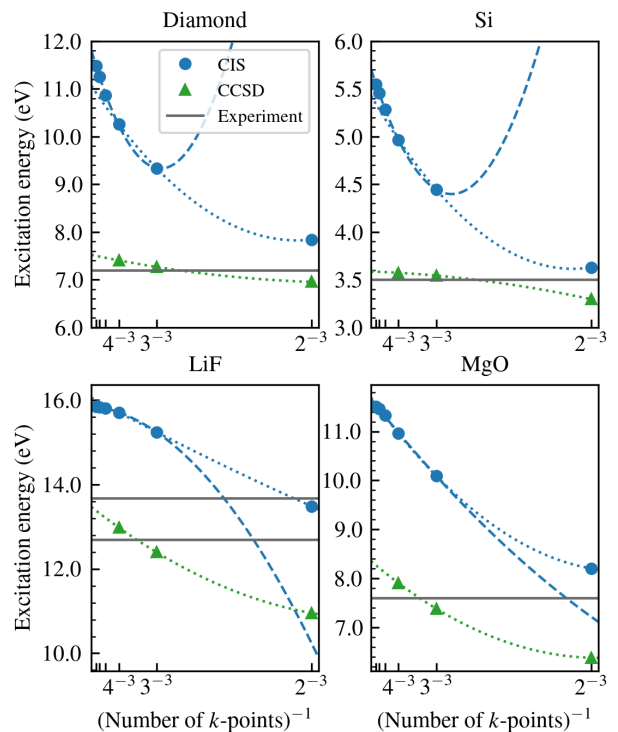


FIG. 2. Excitation energy of diamond, Si, LiF, and MgO calculated with CIS and EOM-CCSD. Results are extrapolated to $N_k \rightarrow \infty$ assuming an error with finite-size scaling as described in the text. The dashed lines are fitted based on results obtained with a number of k -points between 3^3 and 7^3 . The dotted lines include only 2^3 , 3^3 , and 4^3 k -points. A variety of experimental results are indicated by solid lines.

energy of about 11 eV. Second, the excitation energy of AIP has frequently been reported as 3.6 eV, about 1 eV below the EOM-CCSD prediction. A 2019 publication reporting the results of TDDFT and GW/BSE calculations⁹⁶ suggested that the 3.6 eV feature seen in experimental spectra is due to the *indirect* transition of AIP. Experimental spectra show a much stronger peak at around 4.6 eV,⁹⁵ which is the likely value of the first direct excitation energy.

The two materials with the largest error are LiF and MgO. Whereas absorption spectra of LiF typically show a narrow peak at about 12.7 eV⁹⁰ (leading to an overprediction of 0.8 eV), inelastic X-ray scattering data is consistent with a value of 13.68 eV.⁹¹ For MgO, EOM-CCSD overpredicts the excitation energy by about 0.7 eV. This tendency to overestimate excitation energies is the same as the one typically observed in molecules and could potentially be addressed via inclusion of triple excitations. However, we also emphasize that our calculations include no information about finite-temperature or exciton-phonon effects, which are expected to contribute to a reduction in the purely electronic excitation energy.^{98–102}

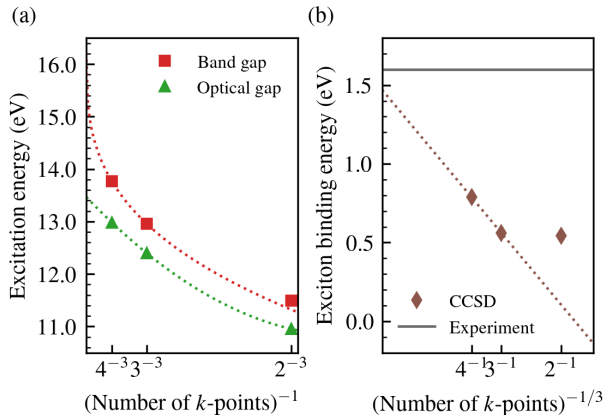


FIG. 3. Fundamental band gap and optical gap (a) and exciton binding energy (b) of LiF from periodic EOM-CCSD. Due to the behavior of IP/EA-EOM-CCSD, the fundamental band gap (red squares) and exciton binding energy (brown diamonds) are extrapolated to $N_k \rightarrow \infty$ assuming a finite-size scaling of the form $E_{N_k} = E_\infty + aN_k^{-1/3}$.

B. Exciton binding energy

We now consider the exciton binding energy, defined as the difference between the fundamental band gap and the first neutral excitation energy (i.e. the optical gap). Within periodic coupled-cluster theory, the band gap is obtained from the calculation of the ionization potential (IP-EOM-CCSD) and the electron affinity (EA-EOM-CCSD), as described in Ref. 52. Here, our IP/EA-EOM-CCSD calculations are basis-set-corrected in the same way as described for our EOM-CCSD calculations.

We focus on LiF, which is a direct-gap ionic insulator with a concomitantly large exciton binding energy. The minimum band gap occurs at the Γ point, which is where we calculate the IP and EA. In Fig. 3(a), we show the fundamental (IP/EA) gap and the optical (EE) gap, as a function of the number of k -points sampled in the Brillouin zone. Clearly the fundamental gap is larger than the optical gap such that the exciton binding energy is positive, as expected. The exciton binding energy is plotted in Fig. 3(b), and seen to be around 0.8 eV with a $4 \times 4 \times 4$ k -point mesh. Unlike neutral excitation energies, which conserve particle number, the IP and EA are charged excitation energies corresponding to a change in particle number. In particular, the same approximation considered above for CIS, i.e. the use of a single determinant, leads to Koopmans' approximation to the ionization potential, $IP \approx -\epsilon_i$; as discussed above, occupied orbital energies converge slowly with N_k when the ERIs are handled as described in section III. Therefore, as shown in Fig. 3(b), we fit the exciton binding energies calculated with $3 \times 3 \times 3$ and $4 \times 4 \times 4$ grids to the form $E(N_k) = E_\infty + aN_k^{-1/3}$, in order to extrapolate to the thermodynamic limit. Doing so gives 1.47 eV, which is in good agreement with the experimental value of 1.6 eV.⁹³ We note that if we separately extrapolate the band gap and the optical gap and take the difference, we get a larger value of 2.74 eV.

C. Exciton dispersion

Although optical absorption spectroscopy and modern theoretical approaches have primarily focused on excitons with $\mathbf{q} = 0$, it is important to also consider excitons that carry a finite momentum \mathbf{q} . For example, electron-hole pairs with finite momentum are realized in many indirect semiconductors and are also important for a quantitative modeling of the exciton-phonon interaction, excitonic dynamics, and radiative lifetimes.

The simulation of excitons with finite-momentum is straightforward in EOM-CCSD, and simply requires that the involved crystal momenta sum to \mathbf{q} in Eqs. 9 and 10. The EOM Hamiltonian is block-diagonal with respect to the exciton momentum and thus all accessible momenta can be studied independently and calculated in parallel. Because the exciton momentum \mathbf{q} corresponds to a momentum difference, a periodic calculation only has access to values $\mathbf{q} = \mathbf{k} - \mathbf{k}'$, where \mathbf{k} are momenta from the k -point mesh. Therefore, different k -point meshes can be utilized in order to access different values of the exciton momentum \mathbf{q} , albeit with an impact on the finite-size error.

Again we focus on LiF, for which we show the EOM-CCSD exciton dispersion in Fig. 4. Our results are compared to inelastic X-ray scattering (IXS) spectroscopy measurements performed by Abbamonte et al.⁹¹ (open circles). We utilize $3 \times 3 \times 3$ k -point mesh (up-pointing triangles) and $4 \times 4 \times 4$ k -point mesh (down-pointing triangles) in order to access more momenta \mathbf{q} in the Brillouin zone. The $3 \times 3 \times 3$ values were rigidly shifted in order to achieve agreement at the Γ point and subsequently, both dispersion data were rigidly shifted in order to place the exciton band center at 14.2 eV, as was observed experimentally.

From their experimental data along the $\Gamma - X$ line, those authors parameterized a tight-binding model (with band center 14.2 eV and nearest-neighbor transfer integral -0.065 eV), which we have extended to the entire Brillouin zone for com-

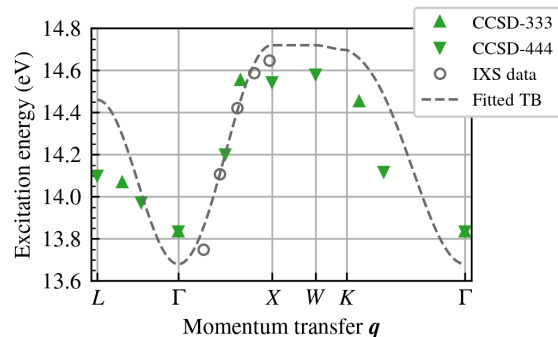


FIG. 4. Exciton dispersion of LiF. Periodic EOM-CCSD data are obtained with different k -point meshes in order to access more values of the momentum transfer \mathbf{q} . Rigid shifts were applied, as described in the text. Also shown are the experimental inelastic X-ray scattering (IXS) data from Ref. 91 and the tight-binding (TB) model fitted to that data.

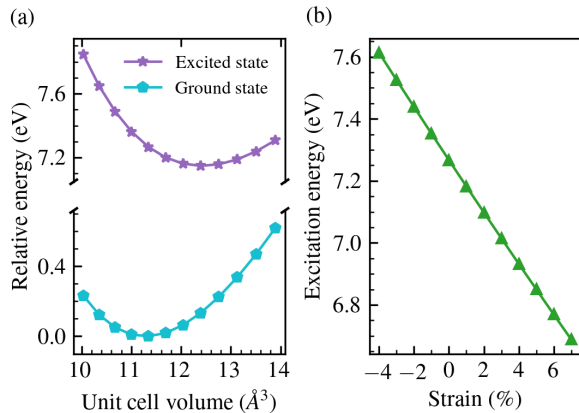


FIG. 5. Ground- and excited-state potential energy surface of diamond as a function of the unit cell volume (a) and the behavior of the excitation energy as a function of hydrostatic strain (b). Results are obtained from CCSD and EOM-CCSD with the DZVP basis set and a $3 \times 3 \times 3$ sampling of the Brillouin zone.

parison (dashed line). We can see that the EOM-CCSD results are in good agreement with the IXS data, with an error less than 0.2 eV along the $\Gamma \rightarrow X$ direction. Our largest discrepancy is at the L point, although we emphasize that experimental data is unavailable at that momentum and the disagreement may indicate a failure of the simple tight-binding model.

D. Exciton-phonon interaction

Finally, we consider the behavior of excitation energies as a function of lattice strain, as predicted by EOM-CCSD. In Fig. 5(a), we show the ground-state and first excited-state potential energy surfaces of diamond, associated with hydrostatic strain, i.e. isotropic variation of the unit cell. While the ground-state energy minimum occurs at a lattice constant of 3.567 \AA (which is fortuitously the exact experimental value^{5,103}), the excited state has a minimum which is shifted to a larger lattice constant of 3.674 \AA .

The behavior of the excitation energy as a function of lattice strain can be used to determine properties of the exciton-phonon interaction. In particular, the interaction with acoustic phonons can be modeled within the deformation potential approximation for the change in the excitation energy,^{104,105}

$\Delta E_X = 3D\varepsilon$, where D is the hydrostatic deformation potential, 3ε is the trace of the strain tensor, $\varepsilon = (a - a_0)/a_0$ is the relative strain, a is the strained lattice constant, and a_0 is the unstrained lattice constant. Defined in this way, our calculations predict the excitonic hydrostatic deformation potential of diamond to be $D = -2.84$ eV. Repeating the same procedure for MgO, we predict a larger $D = -11.73$ eV, indicating a stronger exciton-phonon interaction than in diamond. Experimentally determined deformation potentials for exciton-phonon interactions are sporadic in the literature and we consider a direct comparison on a wider variety of materials to be a topic for future work.

V. CONCLUSIONS

To summarize, we have presented the results of periodic EOM-CCSD for various neutral excited-state properties of semiconductors and insulators. The method has shown promising results for optical excitation energies, exciton binding energies, exciton dispersion relations, and exciton-phonon interaction energies. Collectively, these results demonstrate that EOM-CCSD is a promising and tractable approach for the study of excited-state properties of solids.

While we have attempted to address finite-size errors, arising from incomplete sampling of the Brillouin zone, the high cost of EOM-CCSD precludes a definitive extrapolation. Future work will be focused on both analytical and numerical exploration of finite-size errors and strategies for amelioration, such as those that have been developed for ground-state CCSD.^{51,85,86} In a similar direction, we are exploring the use of approximations to EOM-CCSD with reduced scaling,¹⁰⁶ which will enable the study of simple solids with more k -points or the study of solids with more complex unit cells. Additional future work is targeted at the study of simple metals (where finite-order perturbation theory breaks down¹⁰⁷), the study of exciton-phonon interactions beyond the deformation potential approximation, and the efficient calculation of optical spectra.

ACKNOWLEDGMENTS

X.W. thanks Dr. Varun Rishi for helpful discussions. This work was supported in part by the National Science Foundation under Grant No. CHE-1848369. All calculations were performed using resources provided by the Flatiron Institute. The Flatiron Institute is a division of the Simons Foundation.

* tim.berkelbach@gmail.com

¹ W. Kohn and L. J. Sham, *Phys. Rev.* **140**, A1133 (1965).

² G. Kresse and J. Furthmüller, *Computational Materials Science* **6**, 15 (1996).

³ V. N. Staroverov, G. E. Scuseria, J. Tao, and J. P. Perdew, *Phys. Rev. B* **69**, 075102 (2004).

⁴ J. Paier, M. Marsman, K. Hummer, G. Kresse, I. C. Gerber, and

J. G. ngyn, *J. Chem. Phys.* **124**, 154709 (2006).

⁵ P. Haas, F. Tran, and P. Blaha, *Phys. Rev. B* **79**, 085104 (2009).

⁶ J. K. Nørskov, F. Abild-Pedersen, F. Studt, and T. Bligaard, *PNAS* **108**, 937 (2011).

⁷ K. Burke, *J. Chem. Phys.* **136**, 150901 (2012).

⁸ C. Freysoldt, B. Grabowski, T. Hickel, J. Neugebauer, G. Kresse, A. Janotti, and C. G. Van de Walle, *Rev. Mod. Phys.* **86**, 253

- (2014).
- ⁹ E. Runge and E. K. U. Gross, *Phys. Rev. Lett.* **52**, 997 (1984).
 - ¹⁰ V. I. Gavrilenko and F. Bechstedt, *Phys. Rev. B* **55**, 4343 (1997).
 - ¹¹ I. V. Tokatly and O. Pankratov, *Phys. Rev. Lett.* **86**, 2078 (2001).
 - ¹² L. Reining, V. Olevano, A. Rubio, and G. Onida, *Phys. Rev. Lett.* **88**, 066404 (2002).
 - ¹³ G. Onida, L. Reining, and A. Rubio, *Rev. Mod. Phys.* **74**, 601 (2002).
 - ¹⁴ F. Sottile, F. Bruneval, A. G. Marinopoulos, L. K. Dash, S. Botti, V. Olevano, N. Vast, A. Rubio, and L. Reining, *Int. J. Quantum Chem.* **102**, 684 (2005).
 - ¹⁵ S. Botti, A. Schindlmayr, R. D. Sole, and L. Reining, *Reports on Progress in Physics* **70**, 357 (2007).
 - ¹⁶ J. Paier, M. Marsman, and G. Kresse, *Phys. Rev. B* **78**, 121201 (2008).
 - ¹⁷ A. F. Izmaylov and G. E. Scuseria, *J. Chem. Phys.* **129**, 034101 (2008).
 - ¹⁸ S. Sharma, J. K. Dewhurst, A. Sanna, and E. K. U. Gross, *Phys. Rev. Lett.* **107**, 186401 (2011).
 - ¹⁹ S. Rigamonti, S. Botti, V. Veniard, C. Draxl, L. Reining, and F. Sottile, *Phys. Rev. Lett.* **114**, 146402 (2015).
 - ²⁰ C. A. Ullrich and Z.-h. Yang, “Excitons in time-dependent density-functional theory,” in *Density-Functional Methods for Excited States*, edited by N. Ferré, M. Filatov, and M. Huix-Rotllant (Springer International Publishing, Cham, 2016) pp. 185–217.
 - ²¹ L. Hedin, *Phys. Rev.* **139**, A796 (1965).
 - ²² G. Strinati, H. J. Mattausch, and W. Hanke, *Phys. Rev. Lett.* **45**, 290 (1980).
 - ²³ G. Strinati, H. J. Mattausch, and W. Hanke, *Phys. Rev. B* **25**, 2867 (1982).
 - ²⁴ M. S. Hybertsen and S. G. Louie, *Phys. Rev. Lett.* **55**, 1418 (1985).
 - ²⁵ M. S. Hybertsen and S. G. Louie, *Phys. Rev. B* **34**, 5390 (1986).
 - ²⁶ O. Pulci, M. Marsili, E. Luppi, C. Hogan, V. Garbuio, F. Sottile, R. Magri, and R. D. Sole, *Phys. Status Solidi B* **242**, 2737 (2005).
 - ²⁷ S. Albrecht, L. Reining, R. D. Sole, and G. Onida, *Phys. Status Solidi A* **170**, 189 (1998).
 - ²⁸ W. Hanke and L. J. Sham, *Phys. Rev. B* **21**, 4656 (1980).
 - ²⁹ L. J. Sham and T. M. Rice, *Phys. Rev.* **144**, 708 (1966).
 - ³⁰ G. Strinati, *Phys. Rev. B* **29**, 5718 (1984).
 - ³¹ M. Rohlfing and S. G. Louie, *Phys. Rev. B* **62**, 4927 (2000).
 - ³² A. Georges and G. Kotliar, *Phys. Rev. B* **45**, 6479 (1992).
 - ³³ A. Georges, G. Kotliar, W. Krauth, and M. J. Rozenberg, *Rev. Mod. Phys.* **68**, 13 (1996).
 - ³⁴ A. Georges, *AIP Conference Proceedings* **715**, 3 (2004).
 - ³⁵ G. Kotliar, S. Y. Savrasov, K. Haule, V. S. Oudovenko, O. Parcollet, and C. A. Marianetti, *Rev. Mod. Phys.* **78**, 865 (2006).
 - ³⁶ K. Held, *Adv. Phys.* **56**, 829 (2007).
 - ³⁷ S. Biermann, F. Aryasetiawan, and A. Georges, *Phys. Rev. Lett.* **90**, 086402 (2003).
 - ³⁸ S. Biermann, in *First Principles Approaches to Spectroscopic Properties of Complex Materials*, Topics in Current Chemistry, edited by C. Di Valentin, S. Botti, and M. Cococcioni (Springer Berlin Heidelberg, Berlin, Heidelberg, 2014) pp. 303–345.
 - ³⁹ L. Zhao and E. Neuscamman, *Phys. Rev. Lett.* **123**, 036402 (2019).
 - ⁴⁰ A. J. Williamson, R. Q. Hood, R. J. Needs, and G. Rajagopal, *Phys. Rev. B* **57**, 12140 (1998).
 - ⁴¹ R. J. Hunt, M. Szyniszewski, G. I. Prayogo, R. Maezono, and N. D. Drummond, *Phys. Rev. B* **98**, 075122 (2018).
 - ⁴² Y. Yang, V. Gorelov, C. Pierleoni, D. M. Ceperley, and M. Holzmann, (2019).
 - ⁴³ F. Ma, S. Zhang, and H. Krakauer, *New Journal of Physics* **15**, 093017 (2013).
 - ⁴⁴ J.-Q. Sun and R. J. Bartlett, *J. Chem. Phys.* **104**, 8553 (1996).
 - ⁴⁵ P. Y. Ayala, K. N. Kudin, and G. E. Scuseria, *J. Chem. Phys.* **115**, 9698 (2001).
 - ⁴⁶ C. Pisani, M. Busso, G. Capecchi, S. Casassa, R. Dovesi, L. Maschio, C. Zicovich-Wilson, and M. Schütz, *J. Chem. Phys.* **122**, 094113 (2005).
 - ⁴⁷ M. Marsman, A. Grüneis, J. Paier, and G. Kresse, *J. Chem. Phys.* **130**, 184103 (2009).
 - ⁴⁸ S. Hirata, I. Grabowski, M. Tobita, and R. J. Bartlett, *Chemical Physics Letters* **345**, 475 (2001).
 - ⁴⁹ S. Hirata, R. Podeszwa, M. Tobita, and R. J. Bartlett, *J. Chem. Phys.* **120**, 2581 (2004).
 - ⁵⁰ H. Katagiri, *J. Chem. Phys.* **122**, 224901 (2005).
 - ⁵¹ A. Grüneis, G. H. Booth, M. Marsman, J. Spencer, A. Alavi, and G. Kresse, *J. Chem. Theory Comput.* **7**, 2780 (2011).
 - ⁵² J. McClain, Q. Sun, G. K.-L. Chan, and T. C. Berkelbach, *J. Chem Theory Comput.* (2017).
 - ⁵³ G. H. Booth, A. Grüneis, G. Kresse, and A. Alavi, *Nature* **493**, 365 (2013).
 - ⁵⁴ J. McClain, J. Lischner, T. Watson, D. A. Matthews, E. Ronca, S. G. Louie, T. C. Berkelbach, and G. K.-L. Chan, *Phys. Rev. B* **93**, 235139 (2016).
 - ⁵⁵ A. Pulkin and G. K.-L. Chan, *arXiv:1909.10886* (2019).
 - ⁵⁶ Y. Gao, Q. Sun, J. M. Yu, M. Motta, J. McClain, A. F. White, A. J. Minnich, and G. K.-L. Chan, *arXiv:1910.02191* (2019).
 - ⁵⁷ S. Hirata, M. Head-Gordon, and R. J. Bartlett, *J. Chem. Phys.* **111**, 14 (1999).
 - ⁵⁸ M. Lorenz, D. Usvyat, and M. Schütz, *J. Chem. Phys.* **134**, 094101 (2011).
 - ⁵⁹ M. Lorenz, L. Maschio, M. Schütz, and D. Usvyat, *J. Chem. Phys.* **137**, 204119 (2012).
 - ⁶⁰ A. M. Lewis and T. C. Berkelbach, *Phys. Rev. Lett.* **122** (2019), 10.1103/PhysRevLett.122.226402.
 - ⁶¹ A. M. Lewis and T. C. Berkelbach, *arXiv:1909.11144* (2019).
 - ⁶² F. Coester and H. Kümmel, *Nuclear Physics* **17**, 477 (1960).
 - ⁶³ J. Čížek, *J. Chem. Phys.* **45**, 4256 (1966).
 - ⁶⁴ H. Kümmel, *Theoret. Chim. Acta* **80**, 81 (1991).
 - ⁶⁵ R. J. Bartlett, *Ann. Rev. Phys. Chem.* **32**, 359 (1981).
 - ⁶⁶ R. Bartlett and M. Musiał, *Rev. Mod. Phys.* **79**, 291 (2007).
 - ⁶⁷ K. Emrich, *Nuclear Physics A* **351**, 397 (1981).
 - ⁶⁸ H. Koch and P. Jørgensen, *J. Chem. Phys.* **106**, 8059 (1990).
 - ⁶⁹ J. F. Stanton and R. J. Bartlett, *J. Chem. Phys.* **98**, 7029 (1993).
 - ⁷⁰ R. Kobayashi, H. Koch, and P. Jørgensen, *Chem Phys Lett* **219**, 30 (1994).
 - ⁷¹ A. I. Krylov, *Annu. Rev. Phys. Chem.* **59**, 433 (2008).
 - ⁷² H. J. Monkhorst and J. D. Pack, *Phys. Rev. B* **13**, 5188 (1976).
 - ⁷³ S. Goedecker, M. Teter, and J. Hutter, *Phys. Rev. B* **54**, 1703 (1996).
 - ⁷⁴ C. Hartwigsen, S. Goedecker, and J. Hutter, *Phys. Rev. B* **58**, 3641 (1998).
 - ⁷⁵ J. VandeVondele, M. Krack, F. Mohamed, M. Parrinello, T. Chassaing, and J. Hutter, *Computer Physics Communications* **167**, 103 (2005).
 - ⁷⁶ Q. Sun, T. C. Berkelbach, J. D. McClain, and G. K.-L. Chan, *J. Chem. Phys.* **147**, 164119 (2017).
 - ⁷⁷ F. Oba, A. Togo, I. Tanaka, J. Paier, and G. Kresse, *Phys. Rev. B* **77**, 245202 (2008).
 - ⁷⁸ R. Sundararaman and T. A. Arias, *Phys. Rev. B* **87**, 165122 (2013).
 - ⁷⁹ E. R. Davidson, *J. Comput. Phys.* **17**, 87 (1975).
 - ⁸⁰ K. Hirao and H. Nakatsuji, *Journal of Computational Physics* **45**, 246 (1982).
 - ⁸¹ Q. Sun, T. C. Berkelbach, N. S. Blunt, G. H. Booth, S. Guo, Z. Li,

- J. Liu, J. D. McClain, E. R. Sayfutyarova, S. Sharma, S. Wouters, and G. K.-L. Chan, *WIREs Comput. Mol. Sci.* **8**, e1340 (2018).
- ⁸² P. Carrier, S. Rohra, and A. Görling, *Phys. Rev. B* **75**, 205126 (2007).
- ⁸³ J. Spencer and A. Alavi, *Phys. Rev. B* **77**, 193110 (2008).
- ⁸⁴ A. Grüneis, M. Marsman, and G. Kresse, *J. Chem. Phys.* **133**, 074107 (2010).
- ⁸⁵ G. H. Booth, T. Tsatsoulis, G. K.-L. Chan, and A. Grüneis, *J. Chem. Phys.* **145**, 084111 (2016).
- ⁸⁶ K. Liao and A. Grüneis, *J. Chem. Phys.* **145**, 141102 (2016).
- ⁸⁷ H. R. Phillip and E. A. Taft, *Phys. Rev.* **136**, A1445 (1964).
- ⁸⁸ P. Lautenschlager, M. Garriga, L. Vina, and M. Cardona, *Phys. Rev. B* **36**, 4821 (1987).
- ⁸⁹ S. Logothetidis and J. Petalas, *Journal of Applied Physics* **80**, 1768 (1996).
- ⁹⁰ K. K. Rao, T. J. Moravec, J. C. Rife, and R. N. Dexter, *Phys. Rev. B* **12**, 5937 (1975).
- ⁹¹ P. Abbamonte, T. Graber, J. P. Reed, S. Smadici, C.-L. Yeh, A. Shukla, J.-P. Rueff, and W. Ku, *PNAS* **105**, 12159 (2008).
- ⁹² J. E. Eby, K. J. Teegarden, and D. B. Dutton, *Phys. Rev.* **116**, 1099 (1959).
- ⁹³ D. M. Roessler and W. C. Walker, *J. Opt. Soc. Am.* **57**, 835 (1967).
- ⁹⁴ A. Tararan, S. di Sabatino, M. Gatti, T. Taniguchi, K. Watanabe, L. Reining, L. H. G. Tizei, M. Kociak, and A. Zobelli, *Phys. Rev. B* **98**, 094106 (2018).
- ⁹⁵ S. Hwang, T. Kim, Y. Jung, N. Barange, H. Park, J. Kim, Y. Kang, Y. Kim, S. Shin, J. Song, C.-T. Liang, and Y.-C. Chang, *Journal of Alloys and Compounds* **587**, 361 (2014).
- ⁹⁶ D. Wing, J. B. Haber, R. Noff, B. Barker, D. A. Egger, A. Ramasubramaniam, S. G. Louie, J. B. Neaton, and L. Kronik, *Phys. Rev. Materials* **3**, 064603 (2019).
- ⁹⁷ G. Satta, G. Cappellini, V. Olevano, and L. Reining, *Phys. Rev. B* **70**, 195212 (2004).
- ⁹⁸ A. Marini, *Phys. Rev. Lett.* **101**, 106405 (2008).
- ⁹⁹ F. Giustino, S. G. Louie, and M. L. Cohen, *Phys. Rev. Lett.* **105**, 265501 (2010).
- ¹⁰⁰ G. Antonius, S. Poncé, P. Boulanger, M. Côté, and X. Gonze, *Phys. Rev. Lett.* **112**, 215501 (2014).
- ¹⁰¹ S. Poncé, G. Antonius, Y. Gillet, P. Boulanger, J. Laflamme Janssen, A. Marini, M. Côté, and X. Gonze, *Phys. Rev. B* **90**, 214304 (2014).
- ¹⁰² M. Zacharias, C. E. Patrick, and F. Giustino, *Phys. Rev. Lett.* **115**, 177401 (2015).
- ¹⁰³ C. Kittel, P. McEuen, and P. McEuen, *Introduction to Solid State Physics*, Vol. 8 (Wiley New York, 1996).
- ¹⁰⁴ J. Bardeen and W. Shockley, *Phys. Rev.* **80**, 72 (1950).
- ¹⁰⁵ C. Herring and E. Vogt, *Phys. Rev.* **101**, 944 (1956).
- ¹⁰⁶ J. J. Goings, M. Caricato, M. J. Frisch, and X. Li, *J. Chem. Phys.* **141**, 164116 (2014).
- ¹⁰⁷ J. J. Shepherd and A. Grüneis, *Phys. Rev. Lett.* **110**, 226401 (2013).